Okhotsk Sea and Polar Oceans Research 6 (2022) 19-26

https://doi.org/10.57287/ospor.6.19

Article

Atmospheric warming over the Barents Sea during moisture intrusion events in January 2006. Part II: Impact of sea ice decline

Atsuyoshi MANDA[1]

[1] *Graduate School of Bioresources, Mie University*, *Tsu*, *Japan.*

(Received October 16, 2021; Revised manuscript accepted December 4, 2021)

Abstract

Recent studies suggest the long-term trend of Arctic warming during winter is attributable to increased frequency of occurrence of moisture intrusion events from lower latitudes, but that sea ice loss is also one of the fundamental controlling processes; however, the relative importance of their roles remains disputed. Using numerical simulations, this study examined the impact of sea ice cover on atmospheric warming during moisture intrusion events in January 2006. Atmospheric warming due to sea ice loss could well explain the horizontal distribution of the observed temperature anomaly in January 2006, indicating the importance of sea ice loss in relation to recent Arctic warming. It was found that cooling due to divergence (convergence) of downward (upward) longwave radiation was weakened (enhanced) by sea ice loss, producing a net result of stronger radiative heating. This finding corroborates recent data analysis studies that inferred interaction between sea ice loss and radiative heating. The results indicate that enhanced radiative heating is attributable to changes in the vertical distributions and phases of hydrometeors caused by more unstable near-surface conditions and stronger ascent.

Key words: Arctic amplification; longwave radiation; surface heat flux; polar WRF

1. Introduction

The recent rate of increase in annual air temperatures over the Arctic is twice as fast as that of the global average (Cohen and others, 2014). This warming, which is particularly strong during winter, is referred to as Arctic amplification (AA). Many mechanisms have been proposed to explain AA, some of which include a central role for sea ice loss (*e.g.*, Screen and Simmonds, 2010; Isaksen and others, 2016; Dai and others, 2019). However, other recent studies suggested the importance of moisture intrusion from low latitudes (*e.g.*, Park and others, 2015; Woods and others, 2013, Woods and Caballero, 2016; Gong and others, 2017; Lee and others, 2017). For example, Woods and Caballero (2016) demonstrated that nearly half of the long-term linear trend of 2-m temperature over the Barents Sea could be explained by increased frequency of occurrence of intense moisture intrusion events. They argued that downward longwave radiation (DLR) primarily causes atmospheric warming during these events. Their argument was based on the approximate energy balance of the surface skin layer, which is assumed to have thickness of only a few millimeters. However, the heating mechanism in the air column above the skin layer has yet to be examined fully and it remains unclear.

Manda (2022), hereafter referred to as Part I, examined the heating mechanism in the air column as well as the skin layer during moisture intrusion events in January 2006. The results of that study revealed that DLR at the surface lagged the surface turbulent heat fluxes. Moreover, DLR above the surface diverged and hence contributed to cooling of the air column. These results suggest that DLR was not a primary driver of near-surface warming during the studied intrusion events. It was revealed that vertical diffusion and advection dominated the heating during the events. Condensational heating also contributed to the atmospheric warming but it played a secondary role. It was also demonstrated that another important control in the heating processes was near-surface stability, which is sensitive to both the temperature of air that intrudes into the Barents Sea and the skin temperature over ice and ocean surfaces, suggesting the importance of changes in sea ice cover to atmospheric warming during the events. Substantial reduction in sea ice concentration in the Barents Sea region in January 2006 could impact the overlying atmosphere (Fig. 1).

The objective of this study was to provide more detailed assessment of the impact of sea ice decline on atmospheric warming during the studied moisture intrusion events. As mentioned, the role of sea ice decline in relation to AA remains unclear and disputed. Therefore, the findings of this study contribute to advancing understanding of the mechanism of AA. This study also focused on changes in the interplay between cloud formation and radiation processes, which have not been fully addressed in the previous studies

mentioned above. Such interaction, which remains one of the most important unresolved issues of the Arctic climate system, needs further investigation because this interplay must have substantial impact on AA.

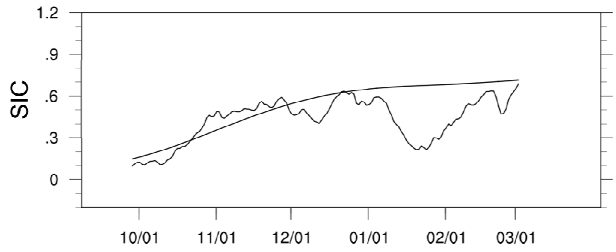

Fig. 1 Time series of sea ice concentration (SIC) averaged over the Barents Sea region (76º–82ºN, 20º–70ºE), derived from European Centre for Medium-Range Weather Forecasts Reanalysis 5th Generation (ERA5) data. Jagged and smoothed lines indicate daily data during 2006/2007 winter and daily climatology, respectively.

Numerical simulations were conducted in this study to investigate the impact of sea ice cover on atmospheric warming. Determination of the impact of sea ice cover from observational data alone is difficult and therefore numerical modeling can be a powerful tool in examination and isolation of the effect of sea ice cover (Higgins and Cassano, 2009; Deser and others, 2010).

2. Data and Method

2.1 Atmospheric model

The atmospheric model used in this study was the same as that adopted in Part I. The polar-optimized Weather Research and Forecasting model (Polar WRF; version 3.7.1), developed by Hines and Bromwich (2008), was used to perform the simulations. European Centre for Medium-Range Weather Forecasts Reanalysis 5th Generation (ERA5) data (Hersbach and others, 2020) were employed for the initial and boundary conditions of the prognostic variables of the model, including sea surface temperature (SST) and sea ice concentration (SIC). The model domain, grid spacings, and subgrid-scale parameterizations were the same as those used in Part I.

2.2 Numerical experiments

To examine the impact of sea ice cover on atmospheric warming, the so-called high ice experiment (HICE) was conducted (Kumar and others, 2010). In this experiment, SICs are specified to be the 1979–2020 daily climatology values. The results from HICE are compared with the output of the simulations conducted in Part I, which hereafter is referred to as the control experiment (CNTL). All input data except for SIC were the same as those used in CNTL. Only SIC was modified to focus on the sole effect of sea ice cover on atmospheric warming, following other previous modeling studies (Magnusdottir and others, 2004; Higgins and Cassano, 2010; Deser and others, 2010). Synoptic-scale atmospheric variations in the Arctic can be affected by many processes, including low-level baroclinicity, static stability (Akperov and others, 2020), and upper-level potential vorticity anomaly (Manda and others, 2020). These processes can complicate the response of the simulated results and could obscure the impact of sea ice cover.

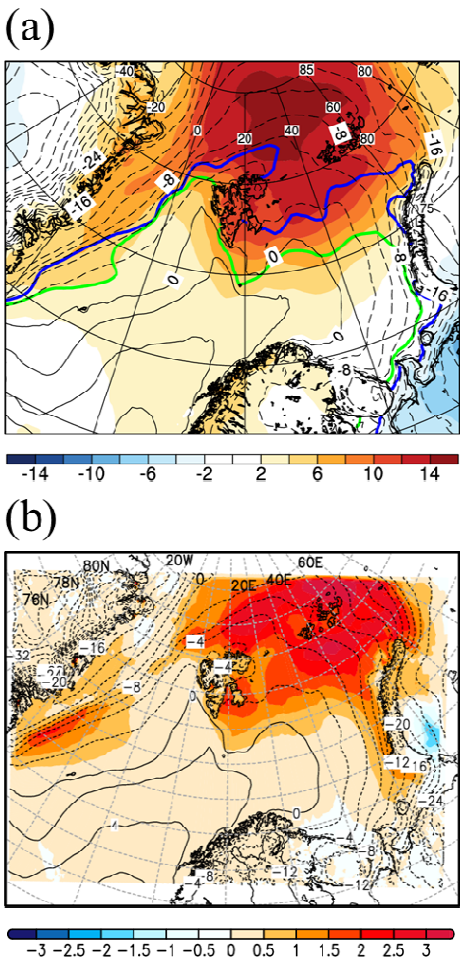

Fig. 2 Horizontal distributions of (a) monthly anomaly of 2-m temperature in January 2006 derived from ERA5 data and (b) difference in 2-m temperature between CNTL and HICE, averaged from January 5–31, 2006. Black contours indicate 2-m temperature. Green and blue contours indicate 20% sea-ice concentrations in January 1979-2020 and 2006, respectively.

As in CNTL, an ensemble experiment was performed to evaluate the uncertainty resulting from internal model variability (Bassett and others, 2020). Each ensemble experiment consisted of five hindcast simulations with different initial times, as described in Part I. The sea ice response is referred as the difference

between the ensemble means of both CNTL and HICE.

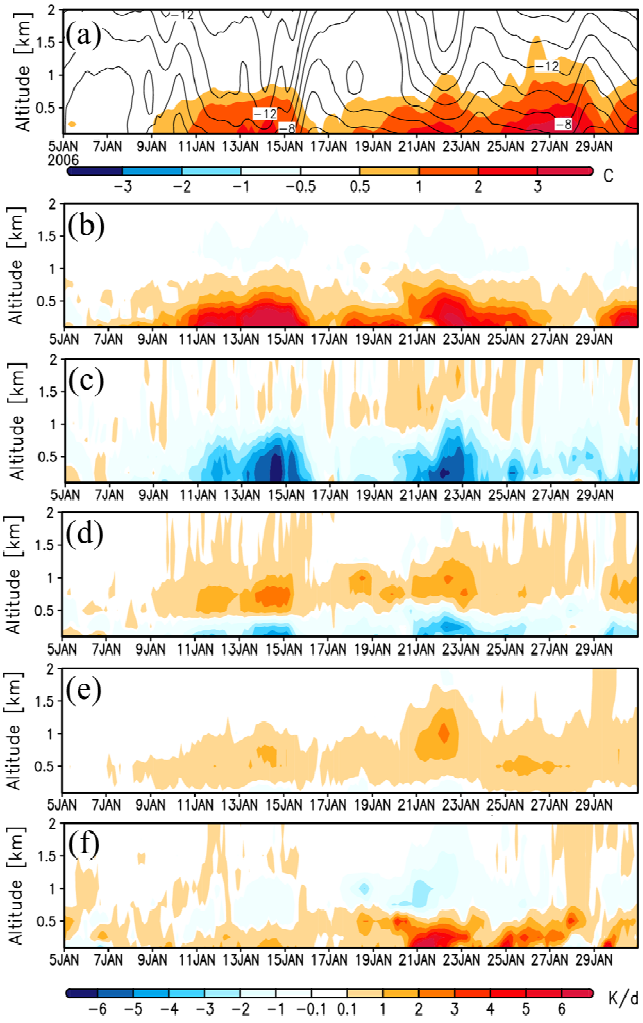

Fig. 3 Time–height cross sections of differences between CNTL and HICE in (a) air temperature, and (b) vertical diffusion, (c) advection, (d) cloud microphysics, (e) cumulus convection, and (f) radiation terms in the thermodynamic energy equation, averaged over the Barents Sea region (76°–82°N, 20°–70°E). Solid contours in (a) indicate the air temperature in CNTL.

3. Results

The horizontal distribution of the monthly anomaly of 2-m temperature in January 2006 from the climatology derived from ERA5 is shown in Fig. 2a, and the differences between the 2-m temperatures in CNTL from those in HICE are shown in Fig. 2b. Although the simulated result (Fig. 2b) underestimates the magnitude of the temperature anomaly in ERA5, the pattern of its spatial distribution is very similar to that of the anomaly in ERA5. The reason for this underestimation is discussed later. Warmer air observed to the north and east of Svalbard and east of Greenland corresponds to regions of substantial sea ice decline, implying that changes in sea ice cover play an important role in determining the spatial pattern of the observed temperature anomaly (Fig. 2a).

Before discussing the differences in heat budgets between CNTL and HICE, main results of the heat budget analyses in CNTL obtained in Part I are summarized here. Near-surface warming (<0.5 km) was primarily due to vertical diffusion acting to transmit the upward SHF (Fig. 7 of Part I). The advection term also contributed to the warming during some periods of January. Condensational heating by the cloud microphysics scheme led to slight cooling just above the surface, whereas the cumulus convection scheme contributed to warming. Net longwave radiation cools the atmosphere due to the divergence of DLR (Fig. 8 of Part I).

The time–height variation of the difference in temperature between CNTL and HICE, averaged over the Barents Sea region (76°–82°N, 20°–70°E; the area enclosed by black lines in Fig. 1a of Part I) is illustrated in Fig. 3a. A high temperature anomaly in CNTL was observed in the lowest 1 km above sea level (ASL).

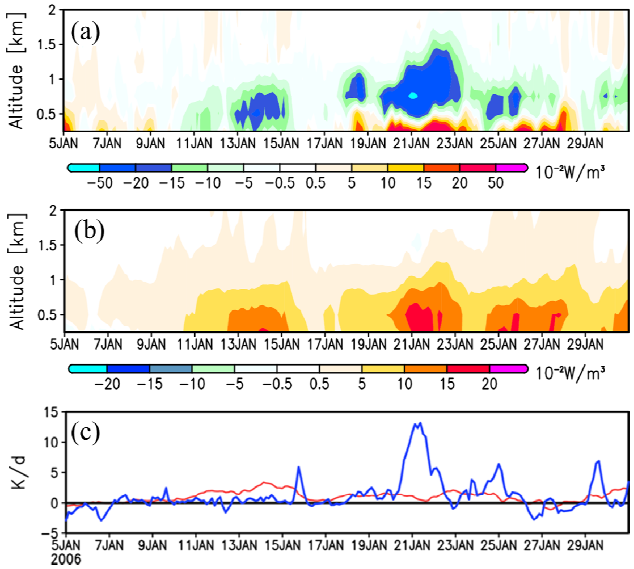

Fig. 4 Same as Fig. 3 but for (a) vertical convergence of (a) DLR and (b) ULR in the air column above 0.1 km ASL. (c) Time series of differences between CNTL and HICE in vertical convergence of ULR (red) and DLR (blue) between the surface and 0.1 km ASL.

The differences in the terms of the thermodynamic energy equation between CNTL and HICE are presented in Fig. 3b–f. The vertical diffusion term dominates the anomalous heating in the lowest 1 km (Fig. 3b), countered by the advection term (Fig. 3c). The radiation term in CNTL is larger than that in HICE (Fig. 3f), meaning that there is less radiative cooling in CNTL relative to that in HICE (see also Fig. 7f in Part I). Heating by the cloud microphysics and cumulus convection schemes in CNTL is also intensified, with

the peak of each elevated from the surface and slightly above that of the radiation term (Fig. 3d and e).

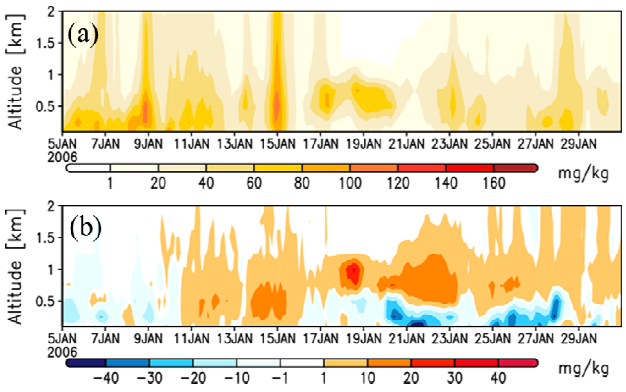

Fig. 5 (a) Same as Fig. 3 but for (a) total mixing ratio in CNTL and (b) its difference between CNTL and HICE.

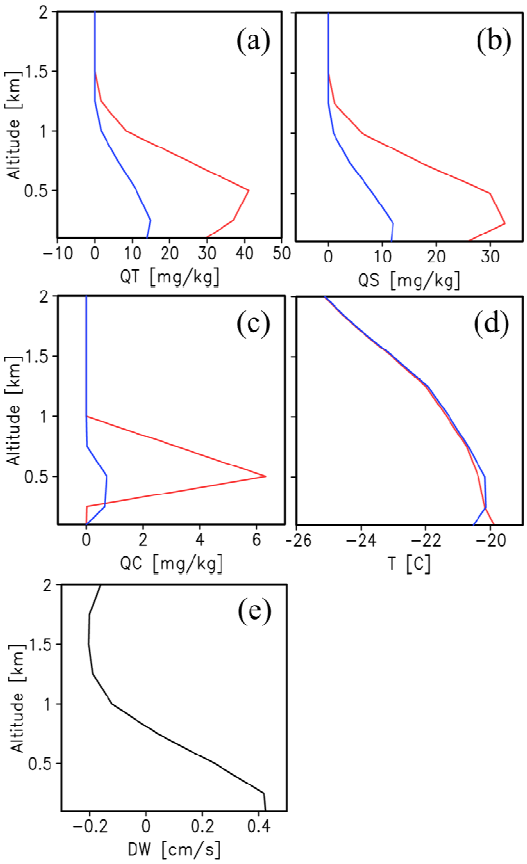

Fig. 6 Vertical profiles of (a) total, (b) snow, and (c) cloud water mixing ratios, and (d) air temperature in CNTL (red) and HICE (blue). (e) Vertical profile of the differences in vertical velocity between CNTL and HICE at 00 UTC on January 14, 2006, averaged over the area 78°–79°N, 60°–65°E.

The time–height cross section of the difference in vertical convergence of DLR between CNTL and HICE above 0.1 km ASL is shown in Fig. 4a. The DLR in CNTL exhibits less divergence than HICE up to approximately 0.5 km ASL during the periods of January 5–10 and January 18–28. During the period of January 11–15, DLR in CNTL was more divergent up to 1 km ASL. However, DLR divergence was slightly weakened below 0.5 km ASL. The convergence of upward longwave radiation (ULR) above 0.1 km ASL intensified during most of the period of the simulation and it extended up to 1 km ASL (Fig. 4b). Both ULR and DLR displayed similar tendencies in the lowest layer below 0.1 km ASL (Fig. 4c). Some peaks of DLR convergence were much larger than those of ULR (*e.g.*, January 21), meaning that sea ice decline led to much stronger near-surface heating by DLR than by ULR in some cases.

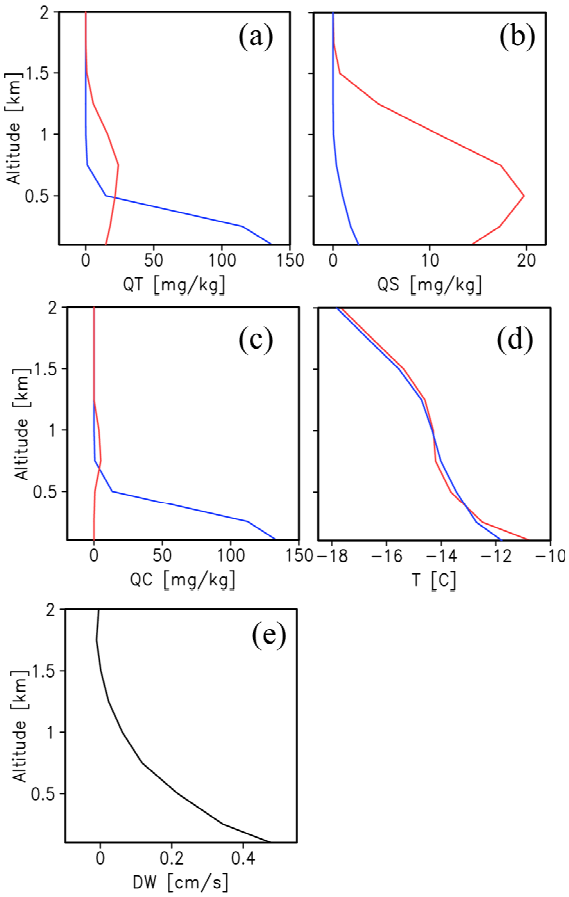

Fig. 7 Same as Fig. 6 but at 00 UTC on January 22, 2006.

These variations in DLR are highly correlated with those in the total mixing ratio, which is defined as the sum of the cloud water and ice, rain, and snow mixing ratios (Fig. 5). The time–height variation of total cloud mixing ratio in CNTL is shown in Fig. 5a. Rapid temperature rises in CNTL around January 9, 15, 23, and 28 (Fig. 3a) correspond well with the local maxima in total mixing ratio shown in Fig. 5a. The total mixing ratio in CNTL exhibits smaller values than in HICE below 0.5 km ASL during the periods of January 5–10

and January 18–28; however, it is larger above 0.5 km ASL during the latter period, indicating upward displacement of hydrometeors (Fig. 5b). Conversely, the total mixing ratio in CNTL is larger than that in HICE from the surface to approximately 1 km ASL during the period of January 11–15.

These spatiotemporal variations of the total mixing ratio can be related to cloud formation processes. Vertical profiles of the total mixing ratio and components (mixing ratios of hydrometeors comprising the total mixing ratio) at 00 UTC on January 14 and 22 are illustrated in Figs. 6 and 7, respectively. The former (latter) corresponds to the period in which DLR in CNTL was more (less) divergent below 0.5 km ASL than in HICE over the Barents Sea region (Fig. 8).

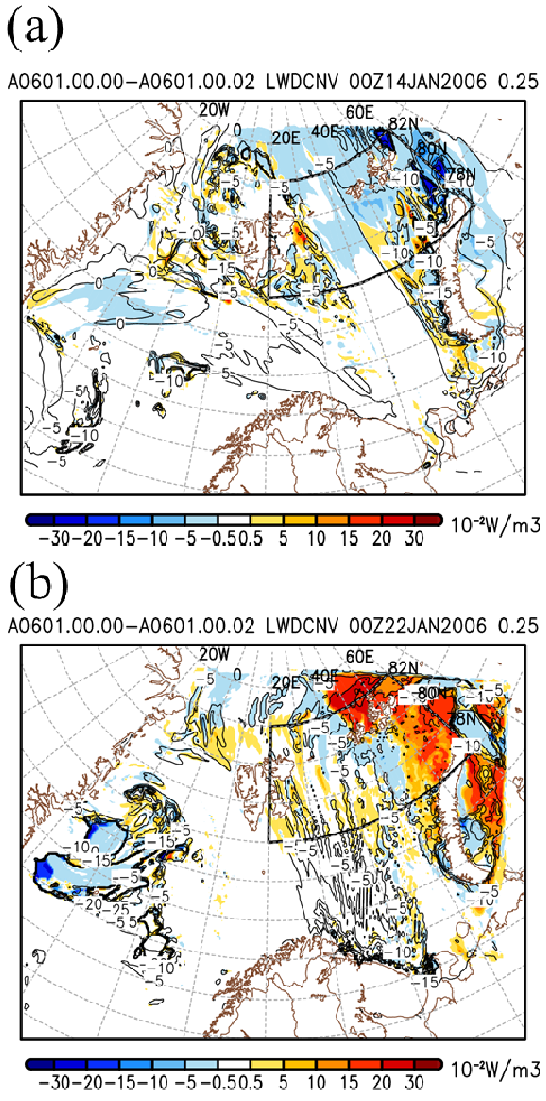

Fig. 8 Maps showing differences in vertical convergence of DLR between CNTL and HICE at 00 UTC on (a) January 14 and (b) January 22, 2006 at 0.25 km ASL (colors). Contours show DLR at 0.25 km ASL in CNTL.

At 00 UTC on January 14, the total mixing ratio in CNTL rapidly increased downward from 1.5 to 0.5 km ASL and then decreased gradually to the surface (red line in Fig. 6a). The total mixing ratio in HICE did not show such prominent vertical variation (blue line in Fig. 6a). The divergence of DLR exhibited large magnitude above 0.5 km ASL, but it became smaller below 0.5 km ASL (Fig. 4a). It should be noted that different areas were taken for computing the averages in Figs. 4 and 6, and that the positive values in Fig. 8a have been smoothed out in Fig. 4.

The major hydrometeor in CNTL was snow at 00 UTC on January 14 (Fig. 6b). The peak of the snow mixing ratio in CNTL was much larger than that in HICE and it was located at approximately 0.3 km ASL. The cloud water mixing ratio in CNTL exhibited a similar distribution, although its peak was slightly higher than that of the snow mixing ratio (Fig. 6c), contributing to an elevated peak of the total mixing ratio (Fig. 6a) and weaker DLR divergence below 0.5 km ASL (Fig. 4a).

Although numerous factors could affect the difference in the mixing ratios between CNTL and HICE, it can be related to differences in the static stability and vertical wind velocity (Fig. 6d and e). The lower troposphere was more unstable and the vertical velocities were relatively larger in CNTL than in HICE, which provided favorable conditions for growth of snow crystals through riming and/or aggregation processes.

At 00 UTC on January 22, the total mixing ratio near the surface in HICE was much larger than in CNTL (Fig. 7a). The cloud water mixing ratio contributed most to the total mixing ratio in HICE (Fig. 7c). The more stable conditions and weaker upward velocity in HICE could support the existence of supercooled water near the surface, which became almost zero in CNTL. Conversely, the snow mixing ratio increased in CNTL (Fig. 7b), and CNTL exhibited more statically unstable conditions and vigorous ascent up to 1 km ASL (Fig. 7d and e), which provided more favorable conditions for growth of ice crystals, as in the case at 00 UTC on January 14.

The enhanced DLR convergence (hence, heating) near the surface (Fig. 8b) can be attributed to differences in the height of the peak of the total mixing ratio between CNTL and HICE. The total mixing ratio in HICE at 00 UTC on January 22 peaked at the lowest layer and monotonically decreased upward (Fig. 7a), which led to strong divergence of DLR near the surface in HICE. In contrast, the total mixing ratio in CNTL peaked at approximately 0.7 km ASL. It indicates that DLR in CNTL was much less divergent and caused much less cooling than in HICE.

Temporal variations of the differences in heat and radiation fluxes at the surface between CNTL and

HICE are illustrated in Fig. 9a. As expected, the sensible and latent heat fluxes and ULR in CNTL were intensified because of the larger areas of open water. Interestingly, DLR was also enhanced in CNTL in comparison with that in HICE. The enhanced surface DLR in CNTL extended further north of the sea ice edge (Fig. 9b), indicating the remote impact of sea ice decline. It also suggests interaction between the turbulent heat fluxes and DLR. Increases in air temperature and moisture due to enhanced turbulent surface heat fluxes could lead to enhancement of DLR at the surface, as suggested in recent data analysis studies (Alexeev and others, 2017; Kim and others, 2019). The results of this study corroborate those findings and suggest new considerations that have not been addressed in previous studies, *e.g.*, the response of the vertical structures of hydrometeors and DLR to sea ice decline.

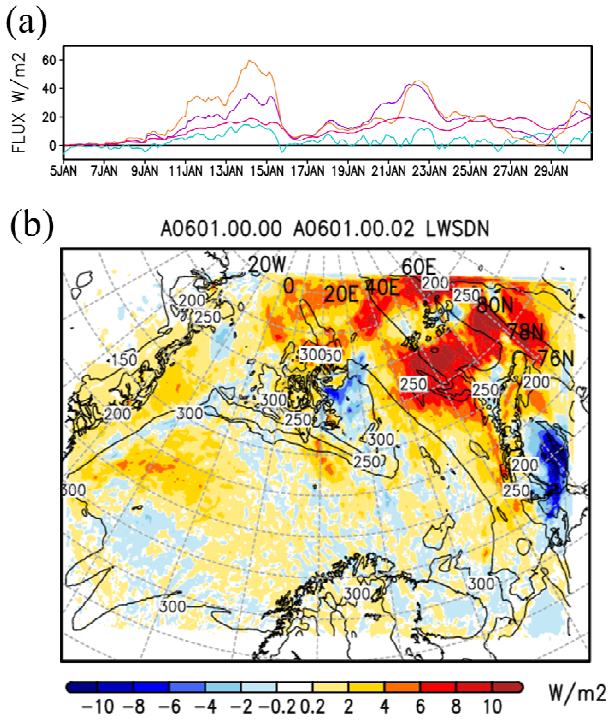

Fig. 9 (a) Time series of differences between CNTL and HICE for sensible heat flux (orange), latent heat flux (purple), ULR (magenta), and DLR (cyan) at the surface. (b) Map showing difference in DLR at the surface between CNTL and HICE averaged from 00 UTC from January 5–31, 2006. Contours indicate DLR in CNTL.

4. Summary and Discussion

The role of sea ice decline in AA remains a matter of debate (Screen and others, 2018). This study demonstrated the impact of sea ice decline on atmospheric warming over the Barents Sea during moisture intrusion events in winter, thereby contributing to advance of the understanding of the mechanism of atmospheric warming in the Barents Sea region, which is the area that shows the most prominent warming in the Arctic.

The changes in sea ice cover in January 2006 well reproduced the horizontal pattern of the observed 2-m temperature anomaly from the climatology, suggesting that sea ice decline has played an important role in the recent warming in the Barents Sea region. Sea ice decline enhances not only the heat and radiative fluxes at the surface but also the radiative and condensational heating in the air column. Under a low ice condition, ULR (DLR) are more convergent (less divergent) than under a high ice condition and hence contribute to the net radiative heating above the surface.

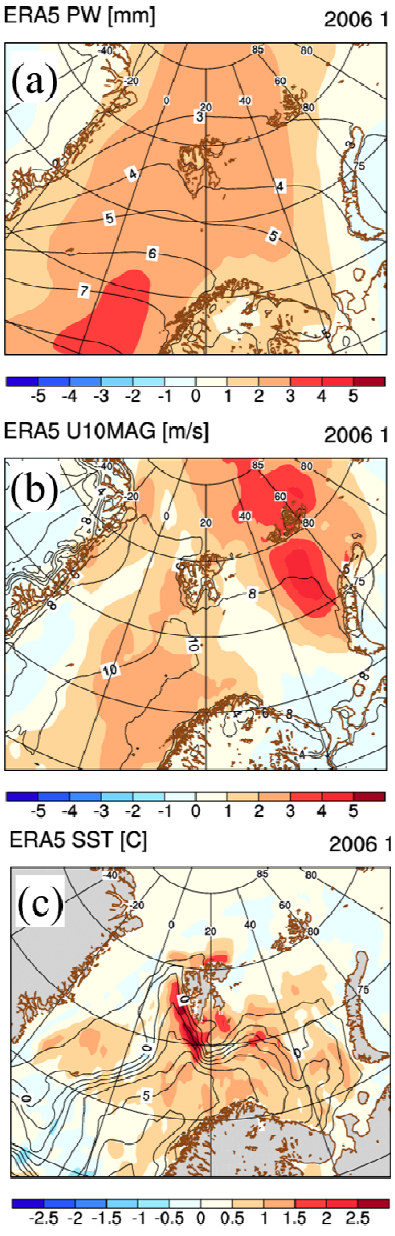

Fig. 10 Horizontal distributions of monthly anomalies of (a) precipitable water, (b) 10-m wind speed, and (c) SST in January 2006 derived from ERA5. Contours indicate the values in CNTL.

The results of this study suggest interaction between radiation and sea ice cover. Enhancement of radiative heating will increase the surface skin temperature, thereby intensifying the sensible heat and latent heat fluxes, which could lead to further enhancement of radiative heating. This study also suggests that changes in DLR are associated with changes in cloud characteristics. Sea ice decline causes more unstable conditions and stronger ascent via enhanced surface fluxes, which change the vertical profiles of hydrometeors and hence DLR.

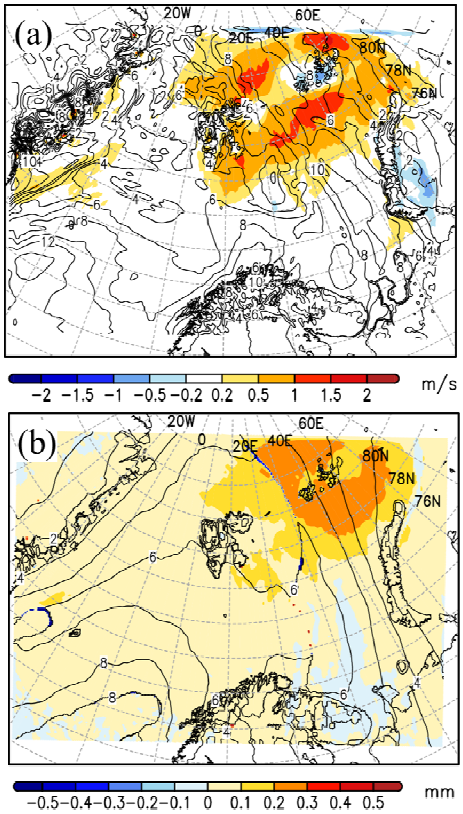

Fig. 11 Same as Fig. 10 but for differences in (a) 10-m wind speed and (b) precipitable water between CNTL and HICE.

Despite the considerable effort to improve the performance of regional Arctic atmospheric models, there are still large intermodel spreads in reproducing the clouds and radiation in the Arctic using different parameterization schemes (*e.g.*, Cassano and others, 2017; Inoue and others, 2021). The modeled responses of hydrometeors and DLR to sea ice decline in this study should be regarded as possible responses of the actual atmosphere. Further observational and/or modeling studies are needed to reduce the uncertainty of the responses in the modeled atmosphere.

This study focused solely on the direct impact of sea ice loss on the magnitude of Arctic warming and its spatial extent during moisture intrusion events, and confirmed that it is the principal factor responsible for the horizontal distribution of observed temperature anomaly. The increase in 2-m temperature in CNTL was much smaller than its anomaly derived from the climatology in ERA5 (Fig. 2). It suggests that other factors should be considered to fully account for the observed temperature anomaly. Various factors could affect the spatiotemporal variation over the Barents Sea region, *e.g.*, the amount of water vapor, wind speed, and SST. In fact, fractional changes from the climatology in observed precipitable water and 10-m wind speed are much larger than the differences in these variables between CNTL and HICE (Figs. 10 and 11), suggesting that anomalous moisture and winds from the climatology contributed to the observed anomalous warming in 2006. Since year-to-year variations of frequency and intensity of the moisture intrusion events are rather large, the analyses in this study should be extended to other years. We note that the atmospheric modeling approach employed in this study is designed to isolate the direct impact of sea ice loss on the atmosphere without accounting for other components of the climate system. The results of this study could be used as a baseline for evaluating the impact of sea ice loss on recent AA. Although various processes can affect atmospheric warming over the Barents Sea region, the responses of the vertical profiles of cloud and DLR to sea ice loss are fundamental to understanding the mechanism of AA.

Acknowledgments

The author thanks Dr. D. H. Bromwich and the Polar Meteorology Group, Byrd Polar and Climate Research Center, Ohio State University for providing the Polar WRF. The author is grateful to Drs. Kazutoshi Sato and Akira Yamauchi for their insightful comments. This work was supported in part by the Arctic Challenge for Sustainability II (ArCS II) Project (Program Grant Number JPMXD1420318865), the Japan Society for Promotion of Science through Grants-in-Aid for Scientific Research (Grant Numbers JP17H02958 and JP19H05697), and the Collaborative Research Program of the Research Institute for Applied Mechanics, Kyushu University (Grant Number 2021 S3-3). The author thanks James Buxton MSc of Edanz (https://jp.edanz.com/ac) for editing a draft of this manuscript.

References

Akperov, M., V.A. Semenov and 4 others (2020): Impact of Atlantic water inflow on winter cyclone activity in the Barents Sea: Insights from coupled regional climate model simulations. *Env. Res. Lett.*, **15**: 024009, doi:10.1088/1748-9326/ab6399.

Alexeev, V.A, J.E. Walsh and 3 others (2017): Warming in the Nordic Seas, North Atlantic storms and thinning Arctic sea ice. *Env. Res. Lett.*, **12**: 084011, doi:

10.1088/1748-9326/aa7a1d.
Bassett, R., P.J. Young and 3 others (2020): A large ensemble approach to quantifying internal model variability within the WRF numerical model. *J. Geophys. Res. Atmos.*, **125**: e2019JD031286.
Cassano, J. J., DuVivier, and 13 others (2017): Development of the regional Arctic system model (RASM): Near-surface atmospheric climate sensitivity, *J. Climate*, **30**: 5729-5753.
Cohen, J. and J. Screen and 9 others (2014): Recent Arctic amplification and extreme mid-latitude weather, *Nat. Geosci.*, **7**: 627–637.
Dai, A., D. Luo and 2 others (2019): Arctic amplification is caused by sea-ice loss under increasing CO_2. *Nat. Commun.*, **10**: 121, doi:10.1038/s41467-018-07954-9.
Dee, D.P., S.M. Uppala and 34 others (2011): The ERA-Interim reanalysis: Configuration and performance of the data assimilation system. *Q.J.R. Meteorol. Soc.*, **137**: 553–597.
Deser, C., R. Tomas and 2 others (2010): The seasonal atmospheric response to projected Arctic sea ice loss in the late twenty-first century. *J. Clim.*, **23**: 333–351.
Gong, T., S. Feldstein, and S. Lee (2017): The role of downward infrared radiation in the recent Arctic winter warming trend, *J. Climate*, **30**: 4937-4949.
Hersbach, H., B. Bell and 42 others (2020): The ERA5 global reanalysis. *Q.J.R. Meteorol. Soc.*, **146**: 1999–2049.
Higgins, M.E. and J.J. Cassano (2010): Response of Arctic 1000 hPa circulation to changes in horizontal resolution and sea ice forcing in the Community Atmospheric Model. *J. Geophys. Res.*, **115**: D17114, doi:10.1029/2009JD013440.
Hines, K.M. and D.H. Bromwich (2008): Development and testing of polar weather research and forecasting (WRF) model. Part I: Greenland ice sheet meteorology. *Mon. Weather Rev.*, **136**: 1971–1989.
Inoue, J., K. Sato and 10 others (2021): Clouds and radiation processes in regional climate models evaluated using observations over the ice-free Arctic Ocean. *J. Geophys. Res*, **126**: e2020JD033904.
Isaksen, K., Ø. Nordli and 4 others (2016): Recent warming on Spitsbergen—Influence of atmospheric circulation and sea ice cover, *J. Geophys. Res*, **121**: 11,913– 11,931.
Kim, K.Y., J.Y. Kim and 5 others (2019): Vertical feedback mechanism of winter Arctic amplification and sea ice loss. *Sci. Rep.*, **9**: 1184, doi:10.1038/s41598-018-38109-x.
Kumar, A., J. Perlwitz and 7 others (2010): Contribution of sea ice loss to Arctic amplification, *Geophys. Res. Lett.*, **37**: L21701, doi:10.1029/2010GL045022.
Lee, S., T. Gong, T. and 3 others (2017): Revisiting the cause of the 1989–2009 Arctic surface warming using the surface energy budget: Downward infrared radiation dominates the surface fluxes. *Geophys. Res. Lett.*, **44**: 10,654– 10,661.
Magnusdottir, G., C. Deser and R. Saravanan (2004): The effects of North Atlantic SST and sea ice anomalies on the winter circulation in CCM3. Part I: Main features and storm-track characteristics of the response. *J. Climate*, **17**: 857–876.
Manda, A., T. Mitsui and 4 others (2020): Storm-mediated ocean–atmosphere heat exchange over the Arctic Ocean: A case study of a Barents Sea cyclone observed in January 2011. *OSPOR*, **4**: 1–9.
Manda, A. (2022): Atmospheric warming over the Barents Sea during moisture intrusion events in January 2006. Part I: Heating mechanism. *OSPOR*, **6**: 7-18.
Park, D.-S., S. Lee and S.B Feldstein (2015): Attribution of the recent winter sea ice decline over the Atlantic sector of the Arctic Ocean, *J. Climate*, **28**: 4027-4033.
Screen, J.A. and I. Simmonds (2010): The central role of diminishing sea ice in recent Arctic temperature amplification. *Nature*, **464**: 1334–1337.
Screen, J.A., C. Deser and 10 others (2018): Consistency and discrepancy in the atmospheric response to Arctic sea-ice loss across climate models. *Nat. Geosci.*, **11**: 155–163.
Woods, C., R. Caballero, and G. Svensson (2013): Large-scale circulation associated with moisture intrusions into the Arctic during winter. *Geophys. Res. Lett.*, **40**: 4717–4721.
Woods, C. and R. Caballero (2016): The role of moist intrusions in winter Arctic warming and sea ice decline, *J. Climate*, **29**: 4473-4485.

Correspondence to: A. Manda, am@bio.mie-u.ac.jp